Available online at www.sciencedirect.com

ScienceDirect

Procedia Structural Integrity 2 (2016) 468–476

Structural Integrity Procedia

www.elsevier.com/locate/procedia

21st European Conference on Fracture, ECF21, 20-24 June 2016, Catania, Italy

Dynamic fracture in rubber toughened polymers: the influence of the fracture surface roughness

Jean-Benoît Kopp[a,*], Christophe Fond[b], Jean Schmittbuhl[c], Olivier Noel[d]

[a] *I2M, Université de Bordeaux, Esplanade des Arts et Métiers, F33400 Talence*
[b] *ICUBE, Université de Strasbourg, 2 rue Boussingault, F67000 Strasbourg*
[c] *EOST, Université de Strasbourg, 5 rue René Descartes, F67000 Strasbourg*
[d] *IMMM, Université du Maine, Avenue Olivier Messiaen, F72085 Le Mans*

Abstract

Dynamic fracture tests have been performed with rubber toughened polymethylmethacrylate (RT-PMMA) samples. For these kinds of materials the macroscopic crack tip velocity $\dot{a} \approx 0.6c_r$ is observed to not change during propagation whatever the available dynamic energy release rate. Therefore dynamic fracture energy values G_{Idc}, according to the crack velocity in a classical formalism, are not unique at the branching velocity (approximately $0.6c_r$). Otherwise the classical formalism considers the amount of created surface during propagation as a flat rectangle (the sample thickness multiplied by the crack length). Nevertheless the RT-PMMA fracture surface roughness are observed to fluctuate as a function of the dynamic energy release rate. The more (respectively less) the dynamic critical energy release rate the rough (respectively smooth) the fracture surface. The real 3D topography of the created surface has to be included in the energy balance to quantify an intrinsic material fracture energy. If not, fracture energy can be significantly underestimated. Using different types of profilometer, the precise amounts of created surfaces for different locations along the fracture were measured both before and after branching at different scales. Since the fracture surface roughness depends on the analysis scale some precautions are requested in the fracture surface analysis. A self-affine geometrical model is introduced using two parameters: the Hurst exponent and the topothesy. The multi-scale description of the fracture surface roughness by a self-affine model is shown to provide a significantly better approximation of the created surface. A new and original geometrical method is introduced to estimate self-affine parameters: the 3D surface scaling method. It is based on the estimate of the amount of created fracture surface using a routine which makes a surface triangulation. Hurst exponents are shown to be unique, $\chi = 0.6 \pm 0.1$ for the different fracture zones and measurement scales. It is shown that topothesy ratios indicate a significant difference of fracture surface roughness amplitude depending on the observation resolution when the detrending technique is not correctly introduced. Indeed, the lower the topothesy, the smoother the fracture surface.

Peer-review under responsibility of the Scientific Committee of ECF21.

Keywords: Dynamic fracture ; polymers ; surface roughness and self-affinity.

* Corresponding author. Tel.: +33 556845392.
E-mail address: jean-benoit.kopp@ensam.eu

Copyright © 2016 The Authors. Published by Elsevier B.V. This is an open access article under the CC BY-NC-ND license (http://creativecommons.org/licenses/by-nc-nd/4.0/).
Peer review under responsibility of the Scientific Committee of ECF21.
10.1016/j.prostr.2016.06.061

1. Introduction

The characterization of polymer fracture is a difficult matter since both viscoplasticity and inertial effects influence the dynamic of fracture (Beguelin et al. (1997, 1998); Ferrer et al. (1998)). Indeed, it has been shown by many authors since the 1970's that the fracture energy of amorphous polymers varies considerably with the crack tip velocity which is in the range of a fraction of Rayleigh waves speed (Fond and Schirrer (1997, 2001a)). Moving cracks have been analytically studied for many years (Broberg (1960); Yoffe (1951); Freund (1972)). It has been demonstrated, considering mode I, that the energy release will vanish for crack tip velocities approaching the Rayleigh waves speed. For a given isotropic material of ρ density, μ shear modulus and ν Poisson's ratio, the Rayleigh waves speed c_r is given with an accuracy of $\pm 0.6\%$ by $c_r \pm \sqrt[2]{\frac{\mu}{\rho}}(0.878 + 0.2\nu - 0.05(\nu + 0.25)^3)$. Otherwise it is admitted that the formalism of Linear Elastic Fracture Mechanics (L.E.F.M.) can be used because of the confinement of the fracture process zone (Kalthoff (1985); Sharon and Fineberg (1999); Mauzac and Schirrer (1992)).

Classically, two kinds of fracture behaviour have been observed concerning rapid crack propagation in materials. On the one hand, there are materials where fracture energy increases with crack tip velocity, typically epoxies, PMMA, PS experimented in the 1970's. In this case, fracture velocity changes during crack propagation according to available energy *i. e.* the dynamic energy release rate G_{Id}. A difference in velocity before and after branching is observed. The main crack propagates faster than the secondary cracks after branching (Williams (1972); Kobayashi et al. (1980); Doll (1976)). This kind of fracture behaviour is generally associated to smooth fracture surface with mirror-like appearance (Fond and Schirrer (2001b)). The amount of created fracture surface during crack propagation is approximated as a flat rectangle typically the crack length times the sample thickness ($T\Delta a$). On the other hand, there are materials where the fracture energy tends to decrease with crack tip velocity. They are viscoplastic blend materials and polymers (Fineberg et al. (1991); Rittel and Maigre (1999)) such as rubber toughened polymethylmethacrylate (RT-PMMA) or many semi-crystallines (Kopp et al. (2014a,b, 2015)). Crack tips for these materials are seen to propagate at the same macroscopic velocity in mode I solicitation no matter the dynamic energy release rate (Fond and Schirrer (2001a); Scheibert et al. (2010); Sharon and Fineberg (1999)). Crack tip velocity is also the same along secondary branches. For these kinds of materials, the amount of created fracture surface evolved with dynamic fracture energy G_{Idc}. The more (respectively less) the dynamic fracture energy the rough (respectively smooth) the fracture surface (Kopp et al. (2013, 2014b, 2015)). As the fracture surface roughness is scale dependant some precautions are requested in the fracture surface analysis. The self-affine geometrical model (Mandelbrot (1982); Bouchaud (1997); Lopez and Schmittbuhl (1998); Schmittbuhl et al. (1995a); Schmittbulh et al. (1995b)) with two parameters (the Hurst exponent and the topothesy) has been widely applied to many natural surfaces including fracture surfaces. This approach is followed in this study to model fracture surface roughness and quantitatively describes its evolution as a function of the analysis scale.

2. Material and methods

2.1. Samples

The industrial grade RT-PMMA used in this study is a blend made of a PMMA matrix containing about twenty percent volume fraction of mono-dispersed spherical elastomer particles of about 100 nm diameter. Rapid crack propagation (RCP) is initiated in such a polymer sample, following the geometry known as a Strip Band Specimen (SBS) geometry (see Fig. 1). The SBS geometry allows a relatively simple mechanical analysis of the structure during a quasi-static regime of propagation. The fracture test is performed using a displacement-controlled Instron tensile testing machine to cancel out, as far as possible, the work done by external forces during RCP. The experimental procedure consists in pre-stressing the sample uniformly placing two samples head to tail render symmetric the loading. Then, the deformation is maintained during a significant time compared to the loading time allowing the relaxation of the sample. The crack is then initiated with a low energy external impact of a razor blade n contact with the notch tip. The entire test is performed at a constant temperature of 23°C. The macroscopic crack velocity is measured using a conductive layer which is sprayed on the sample surface or a high speed camera. A fractured RT-PMMA sample is presented in Fig. 1. Different branching situations are encountered: a macro-branching or a micro-branching. The size of the secondary crack after branching has been used to calculate the difference between these two types of branching.

Macro-branching herein denotes secondary crack extension d typically larger than 1 cm and micro-branching for $d \leq$ 1 cm. The branching (micro- and macro-) of the principle crack appears because of inertial effects at an approximate crack velocity of $0.6c_r$ (Yoffe (1951)). Indeed, inertial effects change the stress field at the crack tip and maximum tension appear in two symmetrical planes in the process zone.

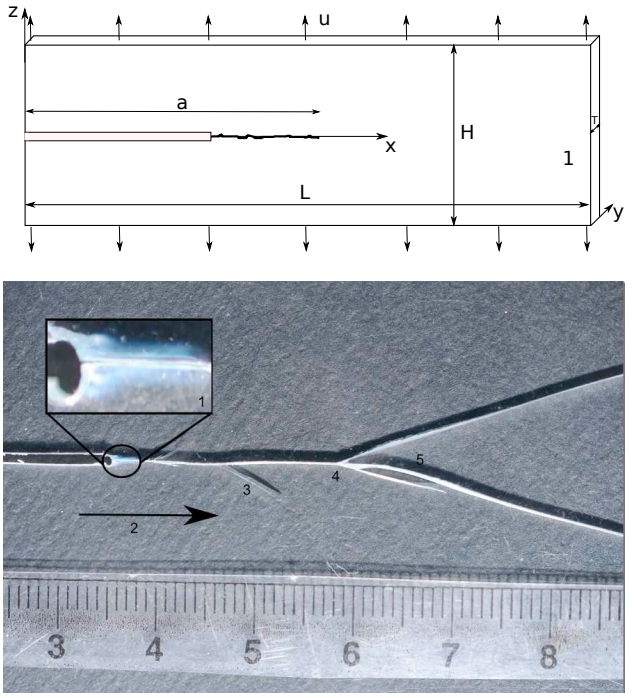

Fig. 1. Sketch of the strip band specimen geometry (SBS) ($L = 200 \pm 1$ mm, $H = 60 \pm 5$ mm, $T = 2 \pm 0.1$ mm) uniformly loaded with imposed displacements u in mode I (top). Post-mortem notched and fractured RT-PMMA sample (bottom): 1-Zoom on the initiation zone where cavitation of rubber particles is visible (whitening of the material around the notch at the initiation of the fracture); 2-Fracture propagation direction; 3-Micro-branching: development of a limited branch ($d < 1$ cm); 4-Macro-branching: development of a significant branch ($d \geq 1$ cm); 5-Fracture kink. For this sample, no conducting layer has been applied.

2.2. Calculation of the mean dynamic energy release rate $< G_{Id} >$

2.2.1. Quasi-static G_{I0}

To estimate the quasi-static energy release rate which is used for reference, it is considered that an increase in crack length Δa corresponds to an elastic unloading of a zone of equivalent length Δa far ahead of the crack tip. This point of view - which allows to consider a plane stress state - leads to an easier calculation than considering the energy released inside the process zone. In a plane stress state ($\sigma_{yy} = 0$), the quasi-static energy release rate G_{I0} is defined as:

$$G_{I0} = \frac{H\sigma_{zz}^2(1-\nu^2)}{2E} \tag{1}$$

where E is the Young modulus of the material corresponding to the unloading rate at the fracture, ν is its Poison ratio, $\frac{H}{2}$ is the half-width of the sample and σ_{zz} is the released stress at the fracture. The corresponding strain follows: $\epsilon_{zz} = \frac{1-\nu^2}{E}\sigma_{zz}$ (Nilsson (1972)).

2.2.2. Dynamic energy release rate G_{Id}

If the crack tip position during propagation $a(t)$ and the stress or strain state at initiation are known, the dynamic energy release rate G_{Id} can be calculated between two crack tip positions a and $a+\Delta a$ by means of a transient dynamic

finite element procedure, using $CASTEM^{©}$ software. G_{Id} is computed assuming a classic Griffith energy balance[1] (Ivankovic et al. (1994); Ferrer et al. (1998); Kopp et al. (2014a)) accounting for inertial effects such as:

$$G_{Id} = \frac{\Delta W_{ext.} - \Delta W_{el.} - \Delta W_{kin.} - \Delta W_{dis.}}{\mathcal{A}_O} \tag{2}$$

where $\mathcal{A}_0$ is the crack area ($\mathcal{A}_0 = T\Delta a$, with T the thickness of the sample), $W_{el.}$ is the elastic energy, $W_{kin.}$ is the kinetic energy, $W_{ext.}$ is the work done by external forces, and $W_{dis.}$ is the bulk dissipated energy integrated into the entire structure. As it has been shown that viscoelasticty outside the process zone is negligible during these experiments, it is assumed that $W_{dis.} \approx 0$ (Fond (2000); Bradley et al. (1997)). A very good agreement with analytical results is obtained with the numerical model (Nilsson (1972)).

A dynamic correction of 10 % in the case of a plate geometry with low border effects at initiation and complete fracture is considered. This correction is significantly lower than the common dynamic correction $(1 - \frac{\dot{a}}{c_r})$, where $\dot{a}$ is the crack tip velocity. Indeed, as explained in (Popelar and Atkinson (1980); Nilsson (1972); Fond (2000)), the geometry of the SBS is known to show lower dynamic correction coefficients (Freund (1972)) and is known to be the best geometry to ensure a regime of propagation close to a steady state (Nilsson (1972)).

2.3. Fracture surface roughness analysis

The fracture surface roughness has been probed at two analysis scales. A prototype of an opto-mechanical stylus profilometer (OMP) developed at EOST was used to characterize the fracture surface at the largest scales. The principle of the OMP consists in probing a fracture surface with a stylus equipped with a sapphire tip of diameter $\phi = 10\,\mu$m located at the end of a mechanical arm allowing the sensing of the topographic variations. To access lower scales, an Interferometric Optical Microscope (IOM) has been used. The principle of the technique (Bruker Contour GT-K1 optical microscope) is based on white light confocal interferometry. The lateral resolution depends on the beam size used for the measurement. In our experiment, the beam size is 195 nm. Roughness data as (x,y,h) files obtained with either OMP or IOM techniques are used to rebuild the topography of fracture surfaces.

3. Results

3.1. Crack tip velocity and $< G_{Id} >$ estimates

During fracture tests, macroscopic crack velocity is observed to be quasi constant all along the propagation of each specimen at a given temperature. The difference in the initial stress $\langle\sigma_{zz}\rangle$ leads to fluctuations in dynamic fracture energy G_{Idc} according to Eq. 2 as shown in Fig. 2. It is interesting that at a given crack tip velocity $\dot{a}$, the dynamic fracture energy G_{Idc} can vary up to 300 %. It is observed that the highest values of G_{Idc} are associated with the roughest surfaces (see Fig. 2-left) while, the lowest values of G_{Idc} are associated with the smoothest surfaces (see Fig. 2-right). $\langle G_{Idc}\rangle_{min}$ is computed as the mean of the minima of G_{Idc} over crack tip velocity. Error bars associated with the average values of $\langle G_{Idc}\rangle$ are estimated as the standard deviation over 8 values for $\langle G_{Idc}\rangle_{max}$ and 3 values for $\langle G_{Idc}\rangle_{min}$ which corresponds respectively to crack propagation configurations *Br.* and *S* (see Table 1).

$\langle G_{Idc}\rangle_{min}$ (kJ/m^2)	$\langle G_{Idc}\rangle_{max}$ (kJ/m^2)	$\langle G_{Idc}\rangle_{max}/\langle G_{Idc}\rangle_{min}$
0.6 ± 0.1	1.70 ± 0.2	3.0 ± 0.2

Table 1. Dynamic fracture energy averaged over time (during a simulated experimentation) for the smallest values: $\langle G_{Idc}\rangle_{min}$, the highest values: $\langle G_{Idc}\rangle_{max}$ and the magnitude of the fluctuations (ratio of maximum over the minimum).

[1] This is equivalent to a contour integral.

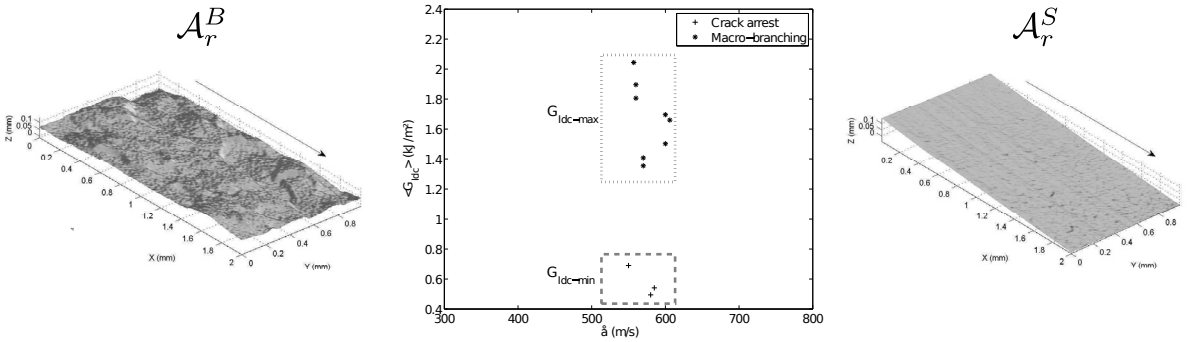

Fig. 2. Center - Dynamic fracture energy G_{Idc} averaged over time during each experiment vs macroscopic crack velocity $\dot{a}$ for 11 experiments. The smallest values of $G_{Idc-min}$ correspond to crack arrest zones and the largest values of $G_{Idc-max}$ correspond to branching zones. Fracture roughness maps of two samples probed by OMP: (left) just before a macro-branching; (right) before a crack arrest along an extended dead branch. Horizontal and vertical scales are identical. The arrow indicates the crack propagation direction.

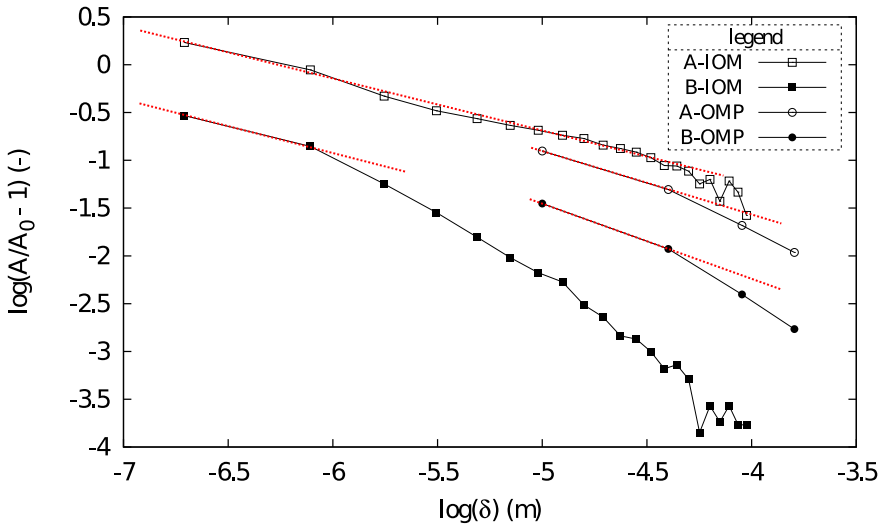

Fig. 3. Evolution of the ratio $\frac{\mathcal{A}_r}{\mathcal{A}_0} - 1$ with the size of the "hypothetical" profilometer tip δ as a function of the measurement scale (OMP and IOM) and the regime (A and B).

3.2. Fracture area measurement and the (2+1)D surface scaling method

A specific approach has been introduced to characterize the fracture surface roughness. It aims at estimating the surface scaling not only from usual extracted 1D profiles but by measuring the scaling of the fracture surface itself. It reinforces the classical (1+1)D estimation of the Hurst exponent value (Schmittbuhl et al. (1995a); Schmittbulh et al. (1995b); Kopp et al. (2015)) in using directly the estimation of the surface area of the fracture surfaces. Indeed, it is based on the estimate of the amount of created fracture surface $\mathcal{A}_r$ and its comparison to the projected area $\mathcal{A}_0$ on the mean fracture plane. With the help of $h(x, y)$ data, a routine makes a triangulation of the surface. In other words, the surface area of the fracture surface is estimated with the sum of each triangular area using three different altitudes. This method of cumulating "triangular" elementary areas has been shown to give similar results as a more precise integration of the surface area by using four nodes interpolation for quadrilateral elements.

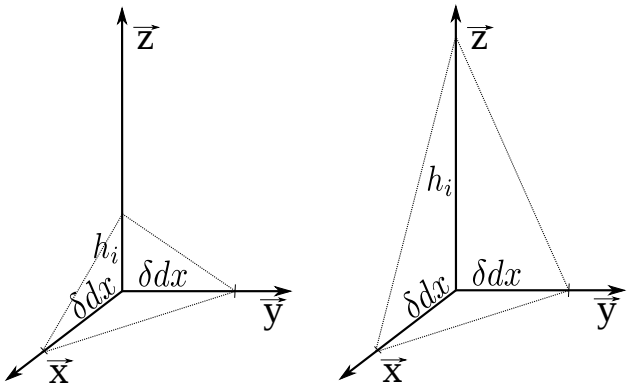

Fig. 4. Two sloping triangular surfaces. Left scheme corresponds to sloping surface for which the approximation $(\frac{h_i}{\delta dx})^2 << 1$ is available contrary to the right scheme. These kinds of sloping surfaces (right) could be observed for fracture surfaces probed near nanometric scale. Indeed, the lower the probe size, the rougher the fracture surface and the more the slope of triangular surface is.

As presented in Table 2, the surface area of the fracture surface depends on the scale measurement. It is observed at OMP scale that the surface area of the fracture surface just before a macro-branching $\mathcal{A}_r^B$ (regime A) is approximately 10 % larger than just before a crack arrest $\mathcal{A}_r^S$ (regime B). At IOM scale this ratio increases up to 210 %.

Technique	d(μm)	$\mathcal{A}_r^B$ / $\mathcal{A}_0$	$\mathcal{A}_r^S$ / $\mathcal{A}_0$	$\mathcal{A}_r^B$ / $\mathcal{A}_r^S$
Opto-mechanical stylus profilometer (OMP)	10	1.11 ± 0.01	1.009 ± 0.002	1.10 ± 0.01
Interferometric Optical Microscope (IOM)	0.195	2.71	1.29	2.10

Table 2. Estimation of the surface area of the fracture surfaces as a function of the resolution technique with d the diameter of the probe. Ratios $\mathcal{A}_r^B/\mathcal{A}_0$ and $\mathcal{A}_r^S/\mathcal{A}_0$ represent normalized surfaces by the projected surface $\mathcal{A}_0$. The ratio $\mathcal{A}_r^B$ / $\mathcal{A}_r^S$ is the relative comparison of surface before branching (regime A) and before arrest (regime B).

Moreover, the routine allows a numerical smoothing of the fracture surface. One method for this reconstruction is used: the convolution method. It consists in computing the convolution of the topography with a sphere (radius δ) that mimics a large probe. The surface area of the fracture surface is then recalculated as a function of δ value. The evolution of $\frac{\mathcal{A}_r}{\mathcal{A}_0} - 1$, where $\mathcal{A}_0$ represents the projected surface, with δ is presented in Fig. 3 for fracture surfaces probed with OMP and IOM before (regime A) and after (regime B) branching.

If it is considered that the triangular area $ds_i(\delta dx, \delta dx, h_i)$ (see Fig. 4) is equal to:

$$ds_i = \frac{1}{2}\sqrt{(\delta dx)^2(\delta dx)^2 + (\delta dx)^2 h_i^2 + (\delta dx)^2 h_i^2} \tag{3}$$

and the triangular area $ds_0(\delta dx, \delta dx, 0) = \frac{1}{2}(\delta dx)^2$. The total area $\mathcal{A}$ represents $\sum_{i=1}^{N} ds_i$:

$$\mathcal{A} = \sum_{i=1}^{N} ds_i = \frac{1}{2}(\delta dx)^2 \sum_{i=1}^{N} \sqrt{1 + 2(\frac{h_i}{\delta dx})^2} \tag{4}$$

It can be approximated $\sqrt{1 + 2(\frac{h_i}{\delta dx})^2} \approx 1 + (\frac{h_i}{\delta dx})^2$ if $(\frac{h_i}{\delta dx})^2 << 1$. Following this condition, and that the projected area $\mathcal{A}_0 = \frac{1}{2}N(\delta dx)^2$, one can obtain:

$$\frac{\mathcal{A}}{\mathcal{A}_0} - 1 = \frac{1}{N}\sum_{i=1}^{N}(\frac{h_i}{\delta dx})^2 \tag{5}$$

It can be noticed that $\sqrt{\frac{1}{N}\sum_{i=1}^{N}(h_i)^2} = l_r^{1-\chi} dx\delta^{\chi}$ (see the Root Mean Square method Kopp et al. (2015); Schmittbulh et al. (1995b)), therefore:

$$\frac{\mathcal{A}}{\mathcal{A}_0} - 1 = \frac{1}{(\delta dx)^2}(l_r^{1-\chi} dx\delta^{\chi})^2 = l_r^{2(1-\chi)} dx\delta^{2(\chi-1)} \tag{6}$$

It can be deduced that:

$$log(\frac{\mathcal{A}}{\mathcal{A}_0} - 1) = 2(1-\chi)log(l_r) + 2(\chi-1)log(\delta) \tag{7}$$

Following this development, Hurst exponent and topothesy values can be deduced from Fig. 3 with a linear regression $y = mx + p$. The slope m is directly linked to the Hurst exponent χ with $m = 2\chi - 2$. It is observed, with this method, that the Hurst exponent value is equal to $\chi = 0.6 \pm 0.1$ (see Table 3) whatever the regime (A and B) and the measurement scale (OMP and IOM) even if a cut-off length seems to appear at large scales for the regime B. This behaviour seems similar to the one highlighted with the classical Root Mean Square method (Kopp et al. (2015)). Topothesies ratios $l_r(A)/l_r(B)$ are respectively equal to 3.9 at OMP scale and 9.2 at IOM scale. Firstly, these results show that the self-affine model provides a good description of the evolution of the fracture area as a function of the measurement resolution. Secondly, it confirms a similarity of the Hurst exponent value for the different regimes (A or B) and the analysis scales, contrary to the topothesy value which is significantly sensitive to the fracture surface roughness. Thirdly, it is observed in Fig. 3 that the self-affine model with χ=0.6 seems no longer convenient at large scales for the regime $B - IOM$. A cut-off length appears at approximately 100 μm. This last observation shows that at large scales, the surface estimate converges toward a flat mean plane.

	OMP	IOM	Average
$\chi(A)$	0.6	0.7	0.6 ± 0.1
$\chi(B)$	0.5	0.6	0.6 ± 0.1

Table 3. Hurst exponent values of RT-PMMA fracture surfaces probed by OMP and IOM for stationary regimes A and B which were obtained using the 3D surface scaling method described in section 3.2.

4. Discussion and conclusions

According to a dynamic Linear Elastic Fracture Mechanics (L.E.F.M.) approach, RT-PMMA samples reveal a loss of unicity of the dynamic fracture energy G_{Idc} at the crack branching velocity (approximately $0.6c_r$) for classical G_{Idc} vs. $\dot{a}$ representation. Indeed, the maximum measured values of the fracture energy are up to 3.0 ± 0.2 times the minimum measured values. The results suggest that the differences of G_{Idc} can be associated to the roughness of the fracture surface which introduces a significant difference between the amount of surface created by fracture $\mathcal{A}_r$ and the projected area on the mean fracture plane $\mathcal{A}_0$. The dynamic fracture energy has until now been estimated as a function of the amount of projected fracture surface $\mathcal{A}_0$, typically the mean flat surface. For RT polymers and semicrystallines (Fond and Schirrer (2001a); Kopp et al. (2013)), the amount of created fracture surface has to be considered in the estimation of G_{Idc}. The scale dependence analysis of RT-PMMA fracture surfaces has led to show the relevance of the self-affine geometrical model which provides a quantification of the surface area of the fracture surface. It is clear that a quantification of "developed rough surface" is of no-sense. Indeed, using continuously decreasing sizes of microscopic probes, one obtains increasing amounts of surface. Nevertheless, the aim of the proposed tool is to explore the possibility to give sense to the estimation of ratios of quantity of created surfaces, the total amount of "seen" surface being describe by a model taking into account the probe size.

A new tool, the 3D surface scaling method, has been developed using Fortran to estimate, first of all, the surface area of the fracture surface $\mathcal{A}_r$ based on a triangulation of the surface. It is noticed for RT-PMMA fractures that $\mathcal{A}_r$ depends on the scale measurement (OMP and IOM) and the regime (A and B). The regime A (respectively B) corresponds to a stationary regime just before a macro-branching (respectively a crack arrest) associated to the roughest (respectively smoothest) surfaces. Secondly, self-affine parameters (Hurst exponent and Topothesy) were estimated. Assuming that $(\frac{h_i}{\delta dx})^2 << 1$, the surface area of the fracture surface can be modelled following the Eq. 3.2.

In this case, the Hurst exponent value is confirmed as staying approximately constant whatever the measurement scale and the regime: $\chi = 0.6 \pm 0.1$. Topothesy values fluctuate as a function of the measurement scale (OMP and IOM) and the regime (A and B). Topothesies (or pre-factors) have highlighted a significant difference of RT-PMMA fracture surface roughness amplitudes, contrary to the Hurst exponent value, as a function of the crack propagation configuration (crack branching and crack arrest). Indeed, the lower the topothesy, the smoother the fracture surface.

To conclude, the self-affine geometrical model with two parameters (Hurst exponent and topothesy) shows its effectiveness in this type of study. However, the single Hurst exponent is no longer sufficient, in itself, to describe all the regimes encountered and, principally, in these kinds of rubber toughened polymer materials. Topothesy values have been shown to be significantly different from one regime to another. Modelling the morphology of the fracture surface roughness with a statistical geometrical model is a practical issue to take into account scaling dependence and to estimate the fracture surface energy. The new guidance in the calculation of the ratio $\frac{\mathcal{A}_r}{\mathcal{A}_0}$ with the self-affine model will be useful in the estimation of the fracture energy. At small scales the model provides a strong dependence contrary to at large scales where it converges to the classically used value $\frac{\mathcal{A}_r}{\mathcal{A}_0}$=1.

References

Beguelin, P. and Fond, C. and Kausch, H.H., 1997. Fracture mechanics at intermediate rates of loading: The influence of the acceleration on compact tension tests 7(C3), Journal de Physique IV, 867–872.

Beguelin, P. and Fond, C. and Kausch, H.H., 1998. The influence of inertial effects on the fracture of rapidly loaded compact tension specimens. part a: Loading and fracture initiation 89(1), International Journal of fracture, 85–102.

Bohme, W. and Kalthoff, J. F, 1985. On the quantification of dynamic in impact loading and the practical application for KId-determination 46(C5), J. Phys. Colloques, C5-213-C5-218.

Bouchaud, E., 1997. Scaling properties of cracks 9(21), Journal of Physics Condensed Matter, 4319–4344.

Bradley, W. and Cantwell, W. and Kausch, H.H., 1997. Viscoelastic creep crack growth: a review of fracture mechanical analyses 1(3), Mechanics Time-Dependant Materials, 241–268.

Borberg, K.B., 1960. The propagation of a brittle crack 18(2), Arkiv fo Fysik, 159–192.

Doll, W., 1976. Application of an energy balance and an energy method to dynamic crack propagation 12(4), Journal of Applied Polymer Science, 595–605.

Family, F. and Vicsek, T., 1985. Scaling of the active zone in the Eden process on percolation networks and the ballistic deposition model 18(2), Journal of Physics A: Mathematical and General, L75–L81.

Feder,J., 1988. Fractals. New York: Plenum Press.

Ferrer, J.-B. and Fond, C. and Arakawa, K. and Takahashi, K. and Beguelin, P. Kausch, H.H. and Mourot, H.H. a, 1998. The influence of crack acceleration on the dynamic stress intensity factor during rapid crack propagation 87(3),Letters in fracture and Micromechanics, 77–82.

Fineberg, J. and Gross, S. and Marder, M. and Swinney, H., 1996. Instability in dynamic fracture 67(4), Phys. Rev. Letters, 457–460.

Fond, C. and Schirrer, R., 1997. Fracture surface energy measurement at high crack speed using a strip specimen: application to rubber toughened PMMA 7(C3), Journal de Physique IV, 969–974.

Fond, C., 2000. Endommagement des polymères “choc”: modélisations micromécaniques et comportements à la rupture, Habilitation à diriger des recherches en mécanique des solides.

Fond, C. and Schirrer, R., 2001. Dynamic Fracture Surface Energy and Branching Instabilities During Rapid Crack Propagation in Rubber Toughened PMMA 329(3), Notes au C.R.A.S., Series IIb, 195–200.

Fond, C. and Schirrer, R., 2001. Influence of crack speed on fracture energy in amorphous and rubber toughened amorphous polymers 30(3), Plast. Rubber Compos., 116–124.

Freund, L.B., 1972. Crack propagation in an elastic solid subjected to general loading-I. Constant rate of extension 20(3), Journal of the Mechanics and Physics of Solids, 129–140.

Irwin, G. and Dally, J. and Kobayashi, T., and Fourney, W. and Etheridge, M. and Rossmanith, H., 1979. On the determination of $\dot{a}$-K relationship for birefringent polymers 19, Experimental mechanics, 121–128.

Ivankovic, A. and Demirdzic, I. and Williams, J. and Leevers, P., 1994. Application of the finite volume method to the analysis of dynamic fracture problems 66(4), International Journal of Fracture,357–371.

Kalthoff, J. F., 1985. On the measurement of dynamic fracture toughnesses ? a review of recent work 27(3), International Journal of Fracture, 277–298.

Kobayashi, A. and Ohtani, N. and Munemura, M., 1980. Dynamic stress intensity factors during viscoelastic crack propagation at various strain rates 25(12), Journal of Applied Polymer Science, 2789–2793.

Kopp, J.-B. and Lin, J. and Schmittbuhl, J. and Fond, C., 2013. Correlation between the dynamic fracture surface energy GID and the amount of created surface 5, International Conference on Fracture 2013 (ICF 2013), 4048–4056.

Kopp, J.-B. and Lin, J. and Schmittbuhl, J. and Fond, C., 2014. Longitudinal dynamic fracture of polymer pipes, European Journal of Environmental and Civil Engineering 18(10), 1097–1105.

Kopp, J.-B. and Schmittbuhl, J. and Noel, O. and Lin, J. and Fond, C., 2014. Fluctuations of the dynamic fracture energy values related to the amount of created fracture surface. Engineering Fracture Mechanics 126, 178–189.

Kopp, J.-B. and Schmittbuhl, J. and Noel, O. and Fond, C., 2015. A self-affine geometrical model of dynamic RT-PMMA fractures: implications for fracture energy measurements, International Journal of Fracture 193(2), 141–152.

Lopez, J. M. and Schmittbuhl, J., 1998. Anomalous scaling of fracture surfaces, Physical Review E 57(6), 6405-6408.

Mandelbrot, B.B., 1982. The Fractal Geometry of Nature, W.H.Freeman and Company (NewYork).

Mauzac, O. and Schirrer, R., 1992. Crack-tip damage zone in rubber toughened amorphous polymers: a micromechanical model 25(12), Journal of Materials Science, 5125–5133.

Morel, S. and Schmittbuhl, J. and Lopez, J. M. and Valentin, G., 1998. Anomalous roughening of wood fractured surfaces 58, Phys. Rev. E, 6999–7005.

Nilsson, F., 1972. Dynamic stress-intensity factors for finite strip problems 8(4), International Journal of Fracture, 403–411.

Ponson, L. and Bonamy, D. and Auradou, H. and Mourot, G. and Morel, S. and Bouchaud, E. and Guillot, C. and Hulin, J.P., 1992. Anisotropic self-affine properties of experimental fracture surfaces 140(1-4), International Journal of fracture, 27–37.

Popelar, C.H. and Atkinson, C., 1980. Dynamic crack propagation in a viscoelastic strip, Journal of the Mechanics and Physics of Solids 28(2), 79–93.

Rittel, D. and Maigre, H., 1996. An investigation of dynamic crack initiation in PMMA, 1996. Mechanics of Materials, 229–239.

Schmittbuhl, J. and Gentier, S. and Roux, S.,1993. Field measurements of the roughness of fault surfaces 20(8), Geophysical research letter, 639–641.

Schmittbuhl, J. and Schmitt, F. and Scholz C., 1995. Scaling invariance of crack surfaces 100(B4), Journal of geophysical research, 5953–5973.

Schmittbuhl, J. and Vilotte, J.-P. and Roux, S., 2015. Reliability of self-affine measurements 51(1), Physical Review E, 131–147.

Scheibert, J. and Guerra, C. and Celarie, F. and Dalmas, D. and Bonamy, D., 2010. Brittle-Quasibrittle Transition in Dynamic Fracture: An Energetic Signature 104, Phys. Rev. Lett., 045501-1–045501-4.

Sharon, E. and Fineberg, J., 1999. Confirming the continuum theory of dynamic brittle fracture for fast cracks 397, Nature, 333–335.

Williams, J. G., 1972. Visco-elastic and thermal effects on crack growth in PMMA 8(4), International Journal of Fracture, 393–401.

H. Yoffe, E., 1951. The Moving Griffith Crack, Philosophical Magazine 42, 739–750.